Journal of Physics:
Condensed Matter

PAPER • **OPEN ACCESS**

High-temperature thermal conductivity of yttrium and rare-earth iron garnets

To cite this article: Makoto Tachibana *et al* 2025 *J. Phys.: Condens. Matter* **37** 405401

OPEN ACCESS
IOP Publishing
Journal of Physics: Condensed Matter
J. Phys.: Condens. Matter **37** (2025) 405401 (7pp)
https://doi.org/10.1088/1361-648X/ae09e6

High-temperature thermal conductivity of yttrium and rare-earth iron garnets

Makoto Tachibana[1,*], **Cédric Bourgès**[2,3] **and Takao Mori**[1,4]

[1] Research Center for Materials Nanoarchitechtonics, National Institute for Materials Science, 1-1 Namiki, Tsukuba 305-0044, Japan
[2] International Center for Young Scientists, National Institute for Materials Science, 1-1 Namiki, Tsukuba 305-0044, Japan
[3] University of Limoges, CNRS, IRCER, UMR 7315, Limoges F-87000, France
[4] Graduate School of Pure and Applied Sciences, University of Tsukuba, 1-1-1 Tennoudai, Tsukuba 305-8577, Japan

E-mail: TACHIBANA.Makoto@nims.go.jp

Received 28 July 2025, revised 5 September 2025
Accepted for publication 22 September 2025
Published 30 September 2025

Abstract

Yttrium and rare-earth iron garnets ($R_3Fe_5O_{12}$) are ferrimagnetic insulators that have been widely studied for magnetic and spintronic applications. In this study, we report the thermal conductivity (κ) between 300 and 773 K for the single crystals of $R_3Fe_5O_{12}$, where R = Y, Gd, Dy, and Yb. For $Y_3Fe_5O_{12}$, the κ up to the Curie temperature ($T_C \approx 555$ K) can be described well with a pure phononic model, without considering conduction or scattering by the magnons. The iron garnets containing magnetic rare-earth ions exhibit smaller κ, with $Dy_3Fe_5O_{12}$ showing the smallest values due to the strong interactions of heat-carrying phonons with the crystal field excitations of Dy^{3+} ions.

Keywords: thermal conductivity, heat capacity, iron garnets, single crystal, phonon, magnon

1. Introduction

The ferrimagnetic insulator $Y_3Fe_5O_{12}$ (yttrium iron garnet or YIG) has been a compound of great importance in spintronics, as its spin waves or magnons possess a long lifetime even at room temperature [1,2]. In 1962−63, thermal conductivity (κ) from magnons was reported for the first time using YIG single crystals [3–5]. These experiments, conducted at liquid helium temperatures, confirmed Sato's earlier prediction [6] that ferro- and ferrimagnetic magnon κ follow a T^2 power law for $T \to 0$ K, unlike the T^3 dependence of the familiar phonon κ. Since the magnon κ can be suppressed under magnetic field, it was also shown that magnon and phonon contributions become comparable in size below ~1 K, while phonons dominate the heat transport at higher temperatures [3–5]. In more recent times, YIG has been used extensively to explore the spin Seebeck effect (SSE) [7, 8], where spin currents are generated from a thermal gradient. It is within this context that the κ of YIG was revisited by various authors, both from experimental [9–13] and theoretical [14–17] perspectives.

YIG is a member of $R_3Fe_5O_{12}$ garnets [18], or *R*IGs, where R can be Y or a rare earth from Sm to Lu. The cubic garnet structure of *R*IGs (space group $Ia\bar{3}d$) is rather complex, with four formula units in the primitive unit cell. The R^{3+} ions, being 8-fold coordinated with oxygen, are located at the c sites. Of the five Fe^{3+} ions in the formula unit, three at the d sites are 4-fold coordinated with oxygen, while two at the a sites are 6-fold coordinated. As a result of antiferromagnetic interactions

* Author to whom any correspondence should be addressed.

between the majority d-site and minority a-site Fe^{3+} ($S = 5/2$) spins, YIG and other *R*IGs undergo a second-order ferrimagnetic transition at a Curie temperature of $T_C \approx 550 - 560$ K [18]. The similar T_Cs found for the entire series indicate that the rare-earth ions, even when magnetic, do not visibly affect the interactions between the Fe^{3+} spins. Nonetheless, the exchange coupling between Fe^{3+} and R^{3+} polarizes the R^{3+} moments below T_C. For R = Gd −Yb there is a compensation temperature below 300 K where the magnetization of the rare-earth ions exactly cancels the net Fe^{3+} magnetization [18]. Recent studies [19–22] have shown that magnetic R^{3+} ions produce features in the SSE that are not found in YIG with the nonmagnetic Y^{3+} ions.

Despite the continuing interest in the iron garnets, especially in regard to the SSE, their κ above room temperature have not been studied in detail. For YIG, much of previous κ studies have focused at low temperatures, where the magnetic field needed to suppress the magnon excitations is experimentally attainable. Though some high-temperature data [10, 23–25] exist, they do not yet provide a clear picture on how the κ evolves below and above the ferrimagnetic transition. As for other *R*IGs, no κ data appears to be available in the literature. These situations thus prompted the present investigation, which reports on the κ between 300 and 773 K for the single crystals of YIG and other *R*IGs (R = Gd, Dy, and Yb, denoted as GdIG, DyIG, and YbIG, respectively). Our data on YIG up to T_C strictly follow the T^{-1} dependence and the values predicted by the Slack equation. These results demonstrate that the κ in this temperature region is fully described by anharmonic phonon-phonon scattering, without any visible contributions from magnon–phonon scattering or magnon heat transport. In contrast, much weaker temperature dependence ($\propto T^{-0.6}$) is found above T_C, suggesting that phonons are scattered from fluctuating Fe^{3+} spins in the paramagnetic phase. Smaller κ are found in other *R*IGs. In particular, DyIG shows the smallest values due to the strong interactions between phonons and the crystal field excitations of Dy^{3+} ions.

2. Experimental details

Since the iron garnets melt incongruently, bulk single crystals are usually grown by a flux method [26] or the floating zone (FZ) method using excess Fe_2O_3 as a solvent [27]. For this study, an FZ-grown YIG crystal was purchased from SurfaceNet GmbH. We also grew single crystals of YIG, GdIG, DyIG, and YbIG using a PbO-PbF_2-B_2O_3 flux [28]. These flux-grown crystals had large {110} faces and their phase purities were confirmed by x-ray powder diffraction. From electron probe microanalysis, small amounts of Pb were detected uniformly in these crystals. Assuming that Pb ions substitute solely the R ions [29], the concentration of Pb at the c site is 1.7% for YIG, 1.2% for GdIG, 1.5% for DyIG, and 0.87% for YbIG. As described below, this study also used a flux-grown single crystal of $Y_3Al_5O_{12}$ (YAG) [30, 31] with an impurity content of Pb/Y = 0.03% [30] and a polycrystalline pellet of $Yb_3Al_5O_{12}$ (YbAG). The YbAG pellet was obtained in a manner similar to that of $Dy_3Al_5O_{12}$ in Tachibana *et al* [32].

The κ between 300 and 773 K was determined from the relation $\kappa = DC_p\rho$, where D is thermal diffusivity, C_p is heat capacity, and ρ is density. D was obtained by the flash method in a nitrogen atmosphere using Netzsch LFA 567. For the measurements, crystals were cut into square plates with 6 ×6 mm^2 faces and ∼1.0 mm thicknesses, and a thin layer of graphite was coated on both sides. The large faces coincided with {110} for the flux-grown *R*IGs and YAG crystals, and {111} for the FZ-grown YIG crystal. The D values have an accuracy of ⩽3% and are shown in the appendix. C_p up to 390 K was measured on smaller samples using the relaxation method of a quantum design physical property measurement system, which has an accuracy of 1% [33]. C_p at higher temperatures was determined as described below. ρ between 300 and 773 K was calculated from literature x-ray values. For YIG, GdIG, YAG, and YbAG, x-ray data up to 773 K are available [34, 35] and these were used to obtain ρ. As only room-temperature x-ray data are available for DyIG and YbIG [36], the thermal expansion of GdIG was adopted for these compounds; this should be justified since $R_3Ga_5O_{12}$ (R = Gd, Dy, and Yb) show nearly identical thermal expansion coefficient at 300 K [37]. Our own ρ measurements at 295 K using the Archimedes method confirmed the x-ray values to within ±1%.

3. Results and discussion

3.1. Heat capacity

We first examine the high-temperature C_p of YIG, which is shown in figure 1. Our present data up to 390 K agree well with those of Devyatkova and Tikhonov [23]. At higher temperatures, there are two sets of data from differential scanning calorimetry (DSC) that provide somewhat conflicting pictures: (1) Uchida *et al*'s C_p [10], while agreeing with our data below 390 K, shows an unusual hump around 500 K. This broad feature appears to be unrelated to the ferrimagnetic ordering of Fe^{3+} spins, since their magnetization data show a sharp transition at T_C = 553 K [10]. Also, their C_p lacks the expected peak at T_C, which leads us to suspect some error in the measurement. (2) Denisov *et al*'s C_p [38] on $Y_{2.93}Ho_{0.07}Fe_5O_{12}$ exhibits a clear peak at T_C, and the overall values at higher temperatures are consistent with those of other iron garnets discussed below. The λ-shape of the peak is consistent with a second-order transition that is strongly affected by critical fluctuations. Although the 2% Ho^{3+} dopant in this sample somewhat broadens the C_p peak, this level of impurity should not significantly affect C_p away from T_C. For $T < T_C$, the most reasonable C_p is obtained by interpolating our data below 390 K and Denisov *et al*'s data above 450 K, which is shown with a red solid line. These values and Denisov *et al*'s C_p above T_C are thus used to obtain the κ for YIG.

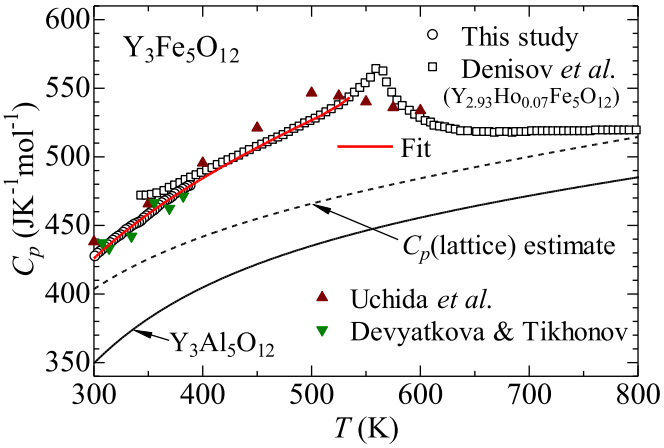

Figure 1. Heat capacity C_p of $Y_3Fe_5O_{12}$. Present data are plotted along with those of Denisov *et al* [38], Uchida *et al* [10], and Devyatkova and Tikhonov [23]. Note that Denisov *et al*'s sample contains Ho^{3+}. The C_p shown with the red solid line is used to obtain thermal conductivity. The black solid line is the C_p of $Y_3Al_5O_{12}$ [39], and the dashed line corresponds to the estimated lattice C_p of $Y_3Fe_5O_{12}$.

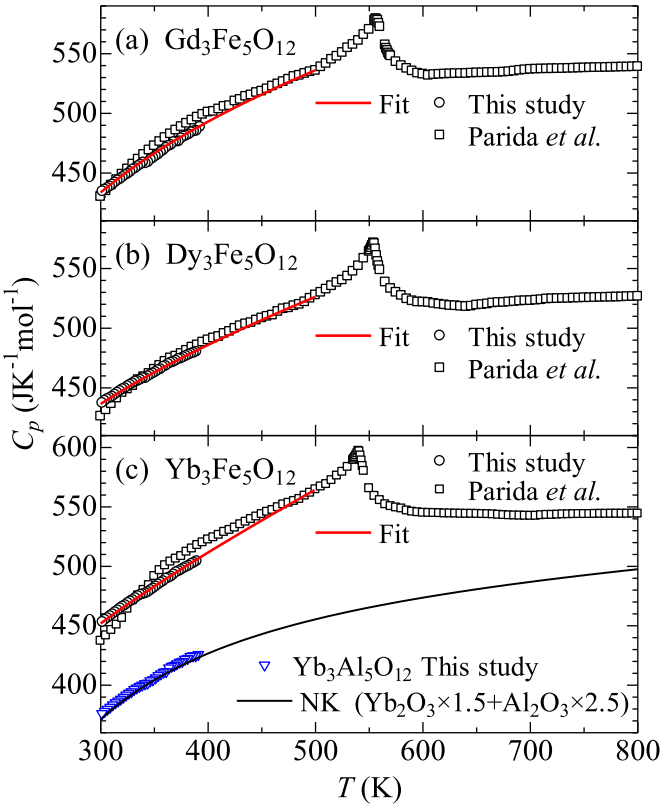

Figure 2. Heat capacity C_p of (a) $Gd_3Fe_5O_{12}$, (b) $Dy_3Fe_5O_{12}$, and (c) $Yb_3Fe_5O_{12}$. Present data are plotted along with those of Parida *et al* [43]. The C_p shown with the red solid lines are used to obtain thermal conductivity. In (c), the C_p of $Yb_3Al_5O_{12}$ from the present study and the Neumann–Kopp (NK) values are also shown.

The black solid line in figure 1 represents the C_p for YAG [39], which is a nonmagnetic isomorph of YIG. The Debye temperature Θ of YAG is 741 K, whereas that of YIG is 560 K [40]. From these data, the lattice C_p for YIG can be roughly estimated by multiplying the temperature scale of C_p for YAG by 560/741 [41], as shown with the dashed line. Bearing in mind the crude nature of this estimate, we obtain the magnetic C_p contribution in YIG at 300 K as 27.4 $JK^{-1}mol^{-1}$. This value is much larger than 2.4 JK^{-1} mol^{-1} calculated from the single parabolic magnon band formula [16, 17], but rather close to 10.3 JK^{-1} mol^{-1} obtained from the 'semi-quantum' calculation using all magnon modes [42]. (The latter predicts T_C = 680 K [42].) Perhaps even better agreement may be achieved if finite temperature effects are fully incorporated into the calculation.

The C_p for other *R*IGs (R = Sm −Lu) have been measured by Parida *et al* using DSC [43]. Their data for GdIG, DyIG, and YbIG are reproduced in figure 2. Compared to YIG, these compounds have slightly larger C_p due to the heavier molecular mass and crystal-field contributions (for Dy^{3+}) from the rare-earth ions. (Θ = 491 K for GdIG [40], while the values are not known for DyIG and YbIG.) The sharp peak at T_C affirms the high quality of the samples. However, Parida *et al*'s C_p contains a shoulder structure near 400 K, an extrinsic feature found in all their data [43]. We thus discard this contribution by extrapolating our C_p to higher temperatures, as shown with the red solid lines. The C_p for YbAG is also presented in figure 2(c). Here, the black solid line refers to the Neumann–Kopp (NK) values, which are obtained by adding the weighted C_p of Yb_2O_3 and Al_2O_3 [44]. The agreement with our experimental data below 390 K is excellent.

3.2. *Thermal conductivity of YIG*

We now discuss heat transport data, starting with those of YIG. The inset of figure 3 shows D near T_C for our FZ crystal, our flux-grown crystal, and Hofmeister's crystal [25] (growth method not specified). In each case, D exhibits a sharp, inverted λ-type dip at T_C, similar in shape to that of sound velocity [45] and signifying interaction of acoustic phonons with the critical fluctuations of the Fe^{3+} spins. There is excellent agreement between our FZ crystal and Hofmeister's crystal, for which $T_C \approx 555$ K can be located. On the other hand, the flux-grown crystal exhibits smaller values of D and T_C (≈535 K), most likely due to the presence of Pb impurity. These results on D are then combined with the C_p in figure 1 to yield three sets of κ data shown in the main panel of figure 3. Due to the sample dependence of C_p, the κ near T_C is plotted with open symbols for our crystals and should be disregarded. However, one may expect the dip in D and the peak in C_p to mirror and cancel each other, as occurs in the κ of ferrimagnetic $NiFe_2O_4$ (T_C = 860 K) [46] and ferromagnetic EuO (T_C = 69 K) [47], for example. As expected for a nonmetallic crystal, the κ of YIG decreases rapidly on heating. The κ at 300 and 773 K for our FZ crystal are 6.6 and 3.0 $Wm^{-1}K^{-1}$, respectively, and nearly identical values are seen for Hofmeister's crystal. Thus,

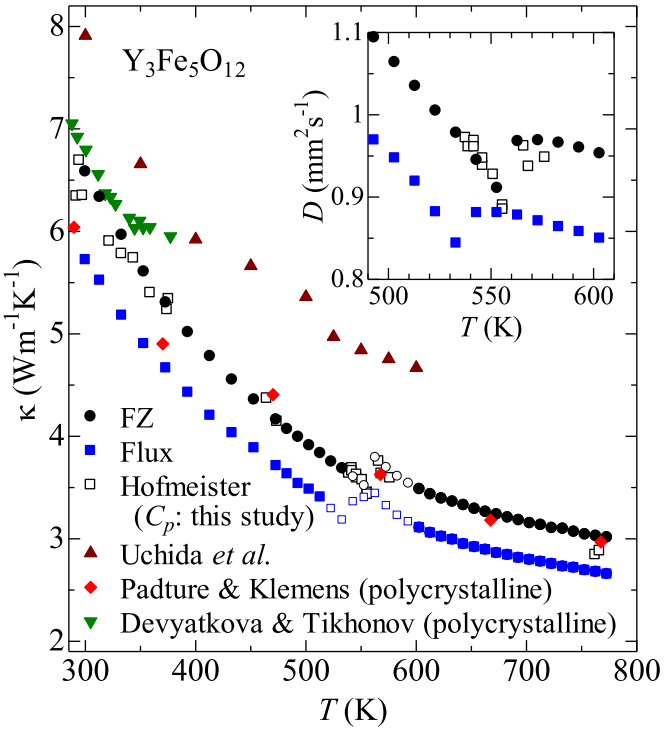

Figure 3. Thermal conductivity κ of $Y_3Fe_5O_{12}$. Present data from the FZ- and flux-grown crystals are plotted along with four sets of published data [10, 23–25]. The κ for Hofmeister is calculated using the C_p obtained in this study. Due to the sample dependence of C_p, κ near the Curie temperature are plotted with open symbols for our crystals. The inset shows thermal diffusivity D near the Curie temperature for the FZ- and flux-grown crystals and Hofmeister's crystal [25].

these data likely represent the κ of high-quality YIG crystals. In contrast, our flux-grown crystal shows ∼10% lower κ values for the entire temperature range, signifying strong phonon scattering from the Pb impurity.

Also shown in figure 3 are the literature κ data from three sources [10, 23, 24]. Two of these [23, 24] were obtained on polycrystalline YIG. Their overall agreement with our single crystal data indicates that the κ is not severely affected by grain-boundary scattering. On the other hand, Uchida *et al.*'s single crystal data [10] exhibit much larger κ, exceeding other values by ∼30% at 600 K. Although the origin of this discrepancy is not clear, it is worth pointing out that both their κ and C_p data (see figure 1) do not show any anomaly at T_C. This indicates that their D (not reported in [10].) also lacks any anomaly at T_C, which is surprising in view of the results shown in the inset of figure 3.

3.2.1 Thermal conductivity below T_C. An important issue to address on YIG is whether magnons play any visible role in the κ at room temperature, either as (1) carriers of heat or (2) scatterers of heat-carrying phonons. In regard to (1), many studies have assumed the magnon κ to be very small, of the order of <0.1 Wm^{-1} K^{-1} at 300 K [16, 17], while two theoretical studies [14, 15] predicted much larger values of 5 and 12 Wm^{-1} K^{-1}, respectively. For (2), various studies reported the evidence of magnon–phonon interactions [8, 48–50], but their impact on κ has not been explored. These questions can be examined from two approaches. First, we evaluate the absolute magnitude of κ using the Slack equation [51, 52]

$$\kappa = \frac{A\bar{M}\delta\Theta^3}{\gamma^2 N^{2/3} T}, \tag{1}$$

where $A = (2.43 \times 10^{-8})/[1 - (0.514/\gamma) + (0.228/\gamma^2)]$, $\bar{M} = 36.9$ u is the mean atomic mass, $\delta = 2.28$ Å is the cubic root of the average volume of each atom, $\Theta = 560$ K is the Debye temperature [40], $\gamma = 1.15$ is the Grüneisen parameter [53], and $N = 80$ is the number of atoms in the primitive unit cell. This equation assumes that only acoustic phonons contribute to the heat transport, and that phonons interact only among themselves via anharmonic three-phonon Umklapp processes [51, 52]. Using the above values, we obtain $\kappa = 6.75$ Wm^{-1} K^{-1} at 300 K, which is nearly identical to the experimental value of 6.6 Wm^{-1}K^{-1}. Since there is some uncertainty in the value of γ [53], the near perfect agreement is most likely fortuitous. Nevertheless, this result clearly shows that a pure phononic model can reproduce the heat transport in YIG at room temperature.

We next evaluate the temperature dependence of κ. In figure 4, the κ of the FZ- and flux-grown YIG are compared with that of nonmagnetic YAG on a log-log scale. For YAG, the best fit to $\kappa = AT^{-\alpha}$ over the entire temperature range yields $\alpha = 1.02$. This is the T^{-1} dependence due to three-phonon scattering processes [54], a feature widely seen in weakly anharmonic insulators and which is captured in the Slack equation. The figure also shows that essentially the same T^{-1} dependence ($\alpha = 1.01$ and 0.97) is found for the two YIG crystals up to T_C. (The slightly smaller α in the flux-grown crystal may arise from the Pb impurity scattering.) Thus, the presence of ferrimagnetically ordered Fe^{3+} spins in YIG has no apparent effect on the temperature dependence of κ, and it is reasonable to conclude that magnons in YIG do not play any significant role as carriers or scatterers of heat from 300 K to T_C. It should be noted that this conclusion does not contradict the observation of the SSE: previous studies have shown that the SSE in YIG is driven mostly by low-energy (<1.5 meV) magnons [9, 17], which constitute only a tiny fraction of the magnons excited at room temperature. Since the majority of thermal magnons have very short mean free paths (<several nm) [9], the total magnon κ can be negligibly small. Moreover, the reported magnon–phonon interactions in YIG occur only at specific positions in the Brillouin zone (the magnon and phonon dispersion crossing points [49] and the Raman-active zone center phonon mode [50]), such that their effects on the overall phonon heat transport can be insignificant. Indeed, no evidence for magnon–phonon interaction was found when the entire magnon spectrum was studied by inelastic neutron scattering [55].

3.2.2 Thermal conductivity above T_C. Figure 4 also shows that the phase transition from the ferrimagnetic state to the paramagnetic state has a strong impact on the κ: for both the FZ- and flux-grown YIG, the obtained $\alpha \approx 0.6$ demonstrates

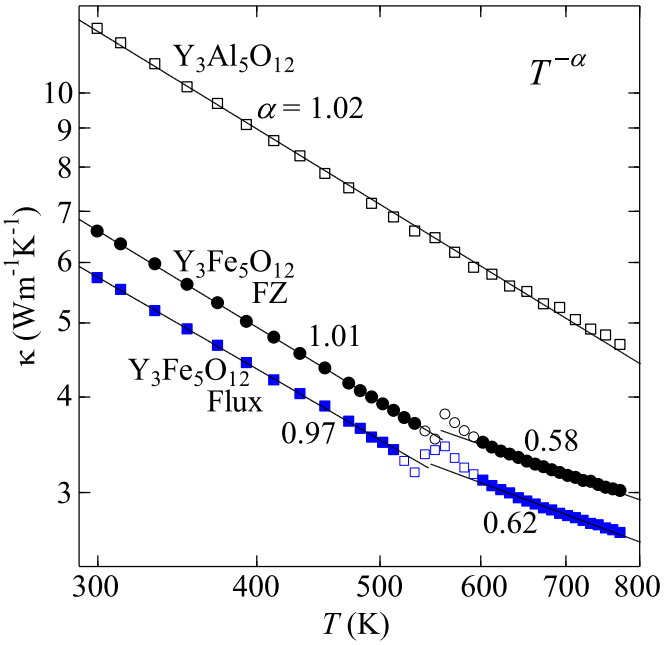

Figure 4. Thermal conductivity κ of $Y_3Al_5O_{12}$ and the FZ- and flux-grown $Y_3Fe_5O_{12}$, plotted in logarithmic scales. The solid lines through the data are fit by $\kappa = AT^{-\alpha}$, and the resulting α are shown.

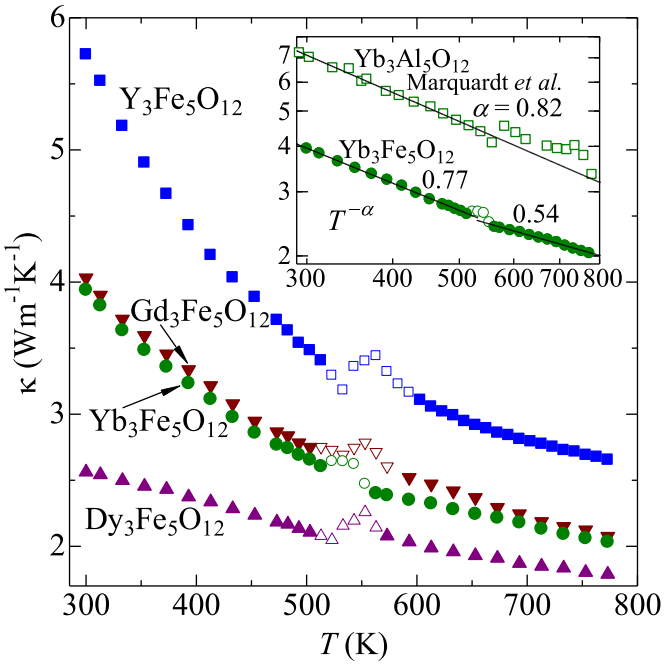

Figure 5. Thermal conductivity κ of flux-grown crystals for $Y_3Fe_5O_{12}$, $Gd_3Fe_5O_{12}$, $Dy_3Fe_5O_{12}$, and $Yb_3Fe_5O_{12}$. The inset plots the κ for $Yb_3Fe_5O_{12}$ and $Yb_3Al_5O_{12}$ in logarithmic scales. The data for $Yb_3Al_5O_{12}$ are obtained from the single-crystal thermal diffusivity of Marquardt *et al* [56] and the C_p in figure 2(c). The solid lines through the data are fit by $\kappa = AT^{-\alpha}$, and the resulting α are shown.

a weaker temperature dependence above T_C. In the paramagnetic phase, the Fe^{3+} spins are no longer ordered and fluctuate randomly, which can become an additional source of phonon scattering. Although similar suppression of κ in the paramagnetic phase is reported for various transition metal oxides [57–59], it is still not clear whether phonons couple directly with fluctuating spins [58] or with the exchange striction induced by spin fluctuations [59]. In this regard, YIG could serve as a simple system to further explore this problem, since the $3d^5$ configuration of Fe^{3+} lacks additional orbital degree of freedom that complicates the problem.

3.3. Thermal conductivity of RIGs

We now move on to discuss heat transport in other iron garnets. Figure 5 shows κ for the flux-grown single crystals of *R*IGs (R = Y, Gd, Dy, and Yb). Due to Pb impurity in these crystals, a small dip in D occurs at a lower temperature than the literature T_C, and there is likely up to ∼10% reduction in κ from the intrinsic values. However, these changes should not significantly affect the relative κ of the four compounds, which is that replacing Y^{3+} with Gd^{3+} or Yb^{3+} reduces the κ at 300 K by ∼30%, whereas replacing with Dy^{3+} reduces the value by 55%. As the difference in cubic lattice parameter is less than 0.8% [18], these results can be attributed to (1) the reduction in average phonon velocity arising from the heavier rare-earth ions ('mass effect') [31, 60], and (2) the reduction in phonon mean free path due to additional scattering from the magnetic moment of rare-earth ions ('magnetic effect'). We note that in *R*IGs, (a) Gd^{3+} has a half-filled 4 f shell ($4f^7$, $^8S_{7/2}$) such that the crystal-field (CF) effects can be neglected, (b) Dy^{3+} ($4f^9$, $^6H_{15/2}$) has eight CF doubles, with six of them thermally populated at 300 K [61], and (c) Yb^{3+} ($4f^{13}$, $^2F_{7/2}$) has the first CF excited state located at ∼550 cm^{-1} (1 cm^{-1} = 1.44 K) [62], such that only the ground-state doublet is populated at 300 K. (Here, we do not consider the additional small splitting due to the exchange field caused by the magnetic ordering of the Fe^{3+} spins [62])

As the three rare-earth ions (Gd^{3+}, Dy^{3+}, and Yb^{3+}) all contain magnetic moments, the mass effect and the magnetic effect cannot be identified separately. However, a comparison between the κ of YAG and LuAG ($Lu_3Al_5O_{12}$) shows that replacing Y^{3+} (89 u) by heavier nonmagnetic Lu^{3+} (175 u) reduces the κ at 300 K from ∼12 to ∼9 Wm^{-1} K^{-1} [63–65], indicating that the mass effect is operative in garnets. Similarly, the magnetic effect can be identified by comparing the κ of LuAG and YbAG [56], since Yb^{3+} (173 u) is similar in mass to Lu^{3+}: as shown in the inset of figure 5, κ = 7.0 Wm^{-1} K^{-1} at 300 K for YbAG is indeed lower than the value in LuAG. The inset also shows that YbAG and the ferrimagnetic phase of YbIG share similar power law behavior with $\alpha \approx 0.8$. This supports the view that the ordered Fe^{3+} spins in YbIG do not significantly affect the thermal transport, as was already seen for YIG. The smaller α (=0.54) found above T_C is also consistent with the result in YIG. Looking now at the main panel of figure 5, we find similar κ values for GdIG and YbIG in the entire temperature range. This is perhaps due to the slightly lighter mass of Gd^{3+} (157 u) being compensated by its spin quantum number S = 7/2, which is larger than the pseudospin value of S = 1/2 in Yb^{3+} [62]. For

GdIG, $\bar{M} = 47.2$ u, $\delta = 2.30$ Å, $\Theta = 491$ K [40], $\lambda = 1.08$ [53], and $N = 80$. Calculating the κ at 300 K with the Slack equation yields 6.65 $Wm^{-1} K^{-1}$, which is much larger than the experimental value of 4.0 $Wm^{-1} K^{-1}$. This result also supports the view that the magnetic moment of Gd^{3+} is involved in the additional scattering of phonons at room temperature.

Compared to other *R*IGs, the κ of DyIG is much smaller and exhibits saturating behavior on cooling. This result is similar to that seen in DyAG ($Dy_3Al_5O_{12}$) [32], where the suppression has been attributed to strong resonant scattering of phonons between the CF levels of Dy^{3+} ions [32, 66, 67]. In DyAG, the low-lying excited doublets are located at 70 and 116 cm^{-1} [66], and detailed calculations [67] showed that excitations between these doublets ($\Delta_{res} = 46$ cm^{-1}) explain the resonant scattering. In DyIG, there are more CF excited levels in the same low-frequency region (at 20, 53, 63, 71, and 87 cm^{-1}) [61], such that similar calculations should reproduce the strongly suppressed κ of this compound. It is interesting to mention that a recent theoretical study [68] has identified CF excitations as an important tuning parameter of the SSE in *R*IGs.

4. Conclusions

We have presented the κ between 300 and 773 K for the single crystals of *R*IGs (*R* = Y, Gd, Dy, and Yb), which provide important insights into the heat transport properties of these compounds. In particular, the results on YIG demonstrate the lack of any visible role of magnons below T_C. This solid experimental finding is a step forward from the discussions in previous studies, where the magnon κ was only assumed to be very small at room temperature. Also, the lower κ found for other *R*IGs underscore the strong effects of rare-earth ions in modifying the heat transport, which should be considered when these compounds are employed in SSE devices.

Data availability statement

All data that support the findings of this study are included within the article (and any supplementary files).

Acknowledgment

We thank M. Nishio for performing the electron probe microanalysis. This study was supported by the funding from JST-Mirai JPMJMI19A1.

Appendix. Thermal diffusivity data

The thermal diffusivity data obtained in this study, which were measured on single crystals using the flash method, are shown in figure A1. A photograph of a YbIG single crystal grown by the flux method is shown in the inset. The large, rhombohedral planes correspond to the {110} faces of the garnet crystal [26].

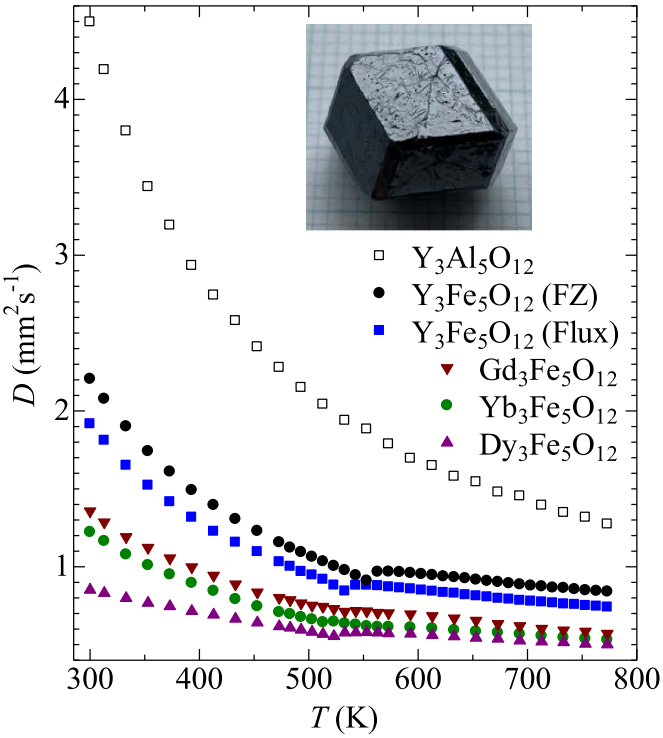

Figure A1. Thermal diffusivity (D) of $Y_3Fe_5O_{12}$, $Gd_3Fe_5O_{12}$, $Dy_3Fe_5O_{12}$, $Yb_3Fe_5O_{12}$, and $Y_3Al_5O_{12}$ single crystals. Data for both the FZ- and flux-grown crystals are shown for $Y_3Fe_5O_{12}$. Other crystals are flux-grown. The inset is a photograph of a flux-grown $Yb_3Fe_5O_{12}$ crystal. Scale in mm.

ORCID iDs

Makoto Tachibana 0000-0002-5907-5563
Cédric Bourgès 0000-0001-9056-0420
Takao Mori 0000-0003-2682-1846

References

[1] Chumak A V, Vasyuchka V I, Serga A A and Hillebrands B 2015 *Nat. Phys.* **11** 453
[2] Serga A A, Chumak A V and Hillebrands B 2010 *J. Phys. D: Appl. Phys.* **43** 264002
[3] Lüthi B 1962 *J. Phys. Chem. Solids* **23** 35–38
[4] Friedberg S A and Harris E D 1962 *Proc. 8th Int. Conf. on Low Temperature Physics* (*Butterworths, London*) p 302
[5] Douglass R L 1963 *Phys. Rev.* **129** 1132
[6] Sato H 1955 *Prog. Theor. Phys.* **13** 119
[7] Uchida K, Ishida M, Kikkawa T, Kirihara A, Murakami T and Saitoh E 2014 *J. Phys.: Condens. Matter* **26** 343202
[8] Kikkawa T and Saitoh E 2023 *Annu. Rev. Condens. Matter Phys.* **14** 129
[9] Boona C S R and Heremans J P 2014 *Phys. Rev. B* **90** 064421
[10] Uchida K, Kikkawa T, Miura A, Shiomi J and Saitoh E 2014 *Phys. Rev. X* **4** 041023
[11] Iguchi R, Uchida K, Daimon S and Saitoh E 2017 *Phys. Rev. B* **95** 174401
[12] Ratkovski D R, Balicas L, Bangura A, Machado F L A and Rezende S M 2020 *Phys. Rev. B* **101** 1744426
[13] Pan B Y, Guan T Y, Hong X C, Zhou S Y, Qiu X, Zhang H and Li S Y 2013 *Europhys. Lett.* **103** 37005

[14] Rezende S M, Rodríguez-Suárez R L, Ortiz J C L and Azevedo A 2014 *Phys. Rev. B* **89** 134406
[15] Costa S S and Sampaio L C 2019 *J. Phys.: Condens. Matter* **31** 275804
[16] Schreier M, Kamra A, Weiler M, Xia J, Bauer G E W, Gross R and Goennenwein S T B 2013 *Phys. Rev. B* **88** 094410
[17] Jamison J S, Yang Z, Giles B L, Brangham J T, Wu G, Hammel P C, Yang F and Myers R C 2019 *Phys. Rev. B* **100** 134402
[18] Gilleo M A 1980 *Ferromagnetic Materials* vol 2, ed E P Wohlfarth (North-Holland) p 1
[19] Geprägs S *et al* 2016 *Nat. Commun.* **7** 10452
[20] Cramer J *et al* 2017 *Nano Lett.* **17** 3334
[21] Kawamoto Y *et al* 2024 *Appl. Phys. Lett.* **124** 132406
[22] Li Y *et al* 2024 *Phys. Rev. Lett.* **132** 056702
[23] Devyatkova E D and Tikhonov V V 1967 *Sov. Phys. Solid State* **9** 604
[24] Padture N P and Klemens P G 1997 *J. Am. Ceram. Soc.* **80** 1018
[25] Hofmeister A M 2006 *Phys. Chem. Miner.* **33** 45
[26] Tachibana M 2017 *Beginner's Guide to Flux Crystal Growth* (Springer)
[27] Kimura S and Shindo I 1977 *J. Cryst. Growth* **41** 192–8
[28] Van Uitert L G, Bonner W A, Grodkiewicz W H, Pictroski M L and Zydzik G J 1970 *Mater. Res. Bull.* **5** 825
[29] Fratello V J, Slusky S E G, Rana V V S, Brandle C D and Ballintine J E 1986 *J. Appl. Phys.* **59** 564
[30] Tachibana M, Iwanade A and Miyakawa K 2021 *J. Cryst. Growth* **568–569** 126191
[31] Tachibana M, Muchtar A R and Mori T 2022 *Phys. Rev. Mater.* **6** 045405
[32] Tachibana M, Bourgès C and Mori T 2023 *Appl. Phys. Express* **16** 061003
[33] Kennedy C A, Stancescu M, Marriott R A and White M A 2007 *Cryogenics* **47** 107
[34] Geller S, Espinosa G P and Crandall P B 1969 *J. Appl. Cryst.* **2** 86–88
[35] Wang X, Xiang H, Sun X, Liu J, Hou F and Zhou Y 2014 *J. Mater. Res.* **29** 2673
[36] Espinosa G P 1962 *J. Chem. Phys.* **37** 2344
[37] Kolmakova N P, Levitin R Z, Orlov V N and Vedernikov N F 1990 *J. Mag. Mag. Mater.* **87** 218
[38] Denisov V M, Denisova L T, Irtyugo L A, Patrin G S, Volkov N V and Chumilina L G 2012 *Phys. Solid State* **54** 2205
[39] Konings R J M, van der Laan R R, van Genderen A C G and van Miltenburg J C 1998 *Thermochim. Acta* **313** 201
[40] Kitaeva V F, Zharikov E V and Chistyi I L 1985 *Phys. Status Solidi a* **92** 475
[41] Gopal E S R 1966 *Specific Heat at Low Temperatures* (Plenum Press)
[42] Barker J and Bauer G E W 2019 *Phys. Rev. B* **100** 140401(R)
[43] Parida S C, Rakshit S K and Singh Z 2008 *J. Solid State Chem.* **181** 101
[44] Barin I 1995 *Thermochemical Data of Pure Substances* (VCH)
[45] Kamilov I K and Aliev K K 1974 *Sov. Phys.–JETP* **38** 954
[46] Nelson A T, White J T, Andersson D A, Aguiar J A, McClellan K J, Byler D D, Short M P and Stanek C R 2014 *J. Am. Ceram. Soc.* **97** 1559
[47] Salamon M B, Garnier P R, Golding B and Buehler E 1974 *J. Phys. Chem. Solids* **35** 851
[48] Kikkawa T, Shen K, Flebus B, Duine R A, Uchida K, Qiu Z, Bauer G E W and Saitoh E 2016 *Phys. Rev. Lett.* **117** 207203
[49] Man H, Shi Z, Xu G, Xu Y, Chen X, Sullivan S, Zhou J, Xia K, Shi J and Dai P 2017 *Phys. Rev. B* **96** 100406(R)
[50] Olsson K S, Choe J, Rodriguez-Vega M, Khalsa G, Benedek N A, He J, Fang B, Zhou J, Fiete G A and Li X 2021 *Phys. Rev. B* **104** L020401
[51] Slack G A 1979 *Solid State Physics* vol 34, ed H Ehrenreich *et al* (Academic) p 1
[52] Morelli D T and Slack G A 2006 *High Thermal Conductivity Materials* ed S L Sindé and J S Goela (Springer) p 37
[53] Saunders G A, Parker S C, Benbattouche N and Alberts H L 1992 *Phys. Rev. B* **46** 8756
[54] Berman R 1976 *Thermal Conduction in Solids* (Oxford University Press)
[55] Pricep A J, Ewing R A, Ward S, Tóth S, Carsten Dubs D P and Boothroyd A T 2017 *npj Quantum Mater.* **2** 63
[56] Marquardt H, Ganschow S and Schilling F R 2009 *Phys. Chem. Miner.* **36** 107
[57] Sun O *et al* 2023 *Mater. Today Phys.* **35** 101094
[58] Sharma P A, Ahn J S, Hur N, Park S, Kim S B, Lee S, Park J-G, Guha S and Cheong S-W 2004 *Phys. Rev. Lett.* **93** 177202
[59] Zhou J-S and Goodenough J B 2002 *Phys. Rev. B* **66** 052401
[60] Wang L-W, Xie L-S, Xu P-X and Xia K 2020 *Phys. Rev. B* **101** 165137
[61] Kang T D, Standard E C, Rogers P D, Ahn K H, Sirenko A A, Dubroka A, Bernhard C, Park S, Choi Y J and Cheong S-W 2012 *Phys. Rev. B* **86** 144112
[62] Peçanha-Antonio V, Prabhakaran D, Balz C, Krajewska A and Boothroyd A T 2022 *Phys. Rev. B* **105** 104422
[63] Kuwano Y, Suda K, Ishizawa N and Yamada T 2004 *J. Cryst. Growth* **260** 159
[64] Aggarwal R L, Ripin D J, Ochoa J R and Fan T Y 2005 *J. Appl. Phys.* **98** 103514
[65] Talik E *et al* 2017 *Mater. Res. Express* **4** 056201
[66] Slack G A and Oliver D W 1971 *Phys. Rev. B* **4** 592
[67] Neelmani and Verma G S 1972 *Phys. Rev. B* **6** 3509
[68] Mori M, Tomasello B and Ziman T 2025 *Phys. Rev. B* **111** 014407